Article

Tuning sol size to optimize organosilica membranes for gas separation☆

Huating Song [1], Yibin Wei [1,2], Chenying Wang [1], Shuaifei Zhao [2,*], Hong Qi [1,*]

[1] State Key Laboratory of Material-Oriented Chemical Engineering, Membrane Science and Technology Research Center, Nanjing Tech University, Nanjing 210009, China
[2] Department of Environmental Sciences, Macquarie University, Sydney 2109, New South Wales, Australia

ARTICLE INFO

ABSTRACT

A series of organosilica sols are prepared by the polymeric sol–gel method using 1, 2-bis(triethoxysilyl)ethane (BTESE) as the precursor. Particle size distributions of the BTESE-derived sols are systematically investigated by carefully adjusting the synthesis parameters (*i.e.*, water ratios, acid ratios and solvent ratios) in the sol process. In certain conditions, increasing the water ratio or the acid ratio tends to cause larger sol sizes and bimodal particle size distributions. However, higher solvent ratios lead to smaller sol sizes and unimodal particle size distributions. The organosilica membranes prepared from the optimized sols show excellent H_2 permeances (up to 4.2×10^{-7} mol·m^{-2}·s^{-1}·Pa^{-1}) and gas permselectivities (H_2/CO_2 is 9.5, H_2/N_2 is 50 and H_2/CH_4 is 68). This study offers significant insights into the relationship between the sol synthesis parameters, sol sizes and membrane performance.

1. Introduction

Recently, amorphous organosilica materials have attracted growing research interest due to their functional characteristics originated from the organic groups in the organic–inorganic hybrid network architecture [1]. They are excellent candidates in membrane preparation because of the desirable characteristics, such as tunable affinity to water [2], easy-to-form films [3], and unique stability under hydrothermal conditions [4,5]. Many precursors, such as alkylene- and aromatic-bridged silsesquioxanes have been selected to fabricate molecule separation membranes. Ethane-bridged silsesquioxane ($(C_2H_5O)_3Si(CH_2)_2Si(OC_2H_5)_3$, BTESE) is one of the most studied precursor molecules [6–9].

The BTESE-derived organosilica membranes have been widely used in various membrane separation technologies, such as pervaporation [4,10–12], gas separation [13–16], reverse osmosis [17] and membrane reactors [18]. Kanezashi *et al.* [16] first developed organosilica membranes by using BTESE as the precursor. BTESE-derived membranes possess better permeabilities than pure silica membranes in gas separation because of the loose networks of the former. The mechanisms have been investigated by molecular dynamics simulation [19] and numerous experimental studies [16,20–22]. Besides, the BTESE-derived membranes

generally have high hydrothermal stabilities. Therefore, organosilica membranes have been considered as good alternatives to pure silica membranes that have poor hydrothermally stabilities.

However, the loose networks of organosilica membranes result in unsatisfactory gas selectivities. To improve gas separation performance of organosilica membranes, four strategies have been proposed in the sol process. The first approach is to adjust the structure of the organic bridge groups. Castricum *et al.* [8] found that organosilica membranes with short alkylene (CH_2 and C_2H_4) bridging groups showed high H_2/N_2 permselectivities. Xu *et al.* [9] reported some microporous organosilica membranes with ethane, ethylene, and acetylene bridges and found that incorporation of rigid bridges into organosilica networks resulted in a looser membrane microstructure. The second method is to control the pore size of organosilica membranes by using the BTESE–TEOS (tetraethoxysilane) mixture as the precursor. The average pore size of the BTESE–TEOS derived membrane is larger than that derived from TEOS, but smaller than that derived from BTESE [22]. Thirdly, doping metals into the organosilica matrix is also an effective method to develop high performance ceramic membranes. Nb and Zr-doping results in denser structures [23–25] and Pd-doping leads to lager micropores [26]. Lastly, optimization of the synthesis parameters of the organosilica sols is the most straightforward approach.

To fabricate membranes with uniform pore size distributions and zero defects, desirable sols should fulfill the following requirements. The particle size of the sols used for coating should fall within a suitable range in which defects caused by penetration of sols into mesopores and cracks resulted from large particles can be avoided. Furthermore, sols should have a narrow particle size distribution that determines the pore size distribution of the derived membranes. The dynamic light

scattering (DLS) technique is widely used as a diagnostic tool for determining the particle size distribution of sols [24,27,28]. Hereinafter, the availability of sol was evaluated using a fast evaluation based on the DLS technique.

In the sol–gel process, a number of parameters, such as the synthesis temperature, reaction time, water ratio (*i.e.* molar ratio of water to the precursor, $n(H_2O):n(BTESE)$), acid ratio (*i.e.* molar ratio of acid to the precursor, $n(H^+):n(BTESE)$) and Si concentration play important roles in sol properties and thus membrane performance. For BTESE and Zr-doped BTESE systems, low synthesis temperatures led to uniform particle size distributions, while high synthesis temperatures resulted in large sol sizes even gelation due to the rise in reaction rates [24]. Long reaction time or high hydrolysis ratios tended to form polydisperse particle size distributions [15]. Increasing Si concentration can also cause large sol sizes [8]. Kreiter *et al.* [29] found that increased acid and water ratios both result in larger particle sizes for BTESE. High acid ratios also lead to sol gelation due to the liquid–liquid immiscibility and cluster formation. Polydisperse particle size distributions and gelation are common issues in the sol–gel process to prepare high performance membranes.

In this work, a careful control of the sol process was applied to minimize the chance of cluster formation. The particle size distribution of the organosilica sol was tuned by adjusting the synthesis parameters, including the water ratio, the acid ratio and the solvent ratio (*i.e.* molar ratio of ethanol to precursor, $n(EtOH):n(BTESE)$) during the sol process. Additionally, sols with suitable particle sizes and narrow particle size distributions were selected to prepare gas separation membranes. Effects of the particle size on membrane performance were investigated by gas permeance experiments.

2. Experimental

2.1. Sol synthesis and characterization

BTESE from ABCR was used as the precursor. Ethanol (anhydrous) was purchased from Merck. Nitric acid (HNO₃, 65 wt%) was purchased from Lingfeng in Shanghai. All chemicals were used as received without further purification.

Organosilica sols were prepared by the following procedure. Briefly, 5 ml BTESE and 5 ml ethanol were well mixed in a glovebox under a nitrogen atmosphere. Meanwhile, 0.54 ml nitric acid solution (1 mol·L⁻¹) was mixed with 5 ml ethanol in a 50 ml beaker and the mixture of HNO₃ aqueous solution and ethanol was then dropwise added into the as-prepared BTESE–ethanol mixture under vigorous stirring (120 r·min⁻¹) in an ice bath. Along with continuous stirring, the final mixture was refluxed in a water bath at 60 °C for 90 min. To obtain homogeneous organosilica sols with different particle size distributions, different amounts of ethanol, water and HNO₃ were investigated and the detailed ingredients in molar ratio are given in Table 1. All organosilica sols were prepared in a clean room and the prepared sol solutions were stored at −16 °C prior to further use.

Particle size distributions of the freshly synthesized sols were measured by a dynamic light scattering analyzer (DLS, Zetatrac, NPA152, Microtrac Inc.) at 30 °C. 1 ml sol was used for every measurement. The particle size distribution and mean particle size of sols were derived from the calculation in the Microtrac software.

2.2. Gel preparation and characterization

Dried flake gels were obtained by drying the corresponding sols for 12 h in petri dishes at room temperature. The obtained gels were then ground into fine powders followed by a thermal treatment under N₂ atmosphere. The thermal treatment procedure included a heating up process at a rate of 0.5 °C·min⁻¹, heat preservation for 3 h at 400 °C and subsequently a cooling down process at a rate of 0.5 °C·min⁻¹.

Table 1
Molar ratio of the ingredients for the synthesis of organosilica sols

Sol	$n(EtOH):n(BTESE)$	$n(H_2O):n(BTESE)$	$n(H^+):n(BTESE)$
1	13.08	2.29	0.04
2		5.56	
3		11.16	
4		22.24	
5	13.08	3.44	0.06
6			0.08
7			0.09
8			0.12
9	19.62	22.24	0.04
10			0.08
11			0.1
12			0.12
13			0.16
14	26.12	22.24	0.2
15			0.3
16			0.4
17	6.54	22.24	0.04
18	26.16		

Thermal behaviors of the organosilica powders were evaluated by a thermogravimetric analysis (TGA) apparatus (STA-449-F3, Netzsch) with a heating rate of 10 °C·min⁻¹ from room temperature to 800 °C under N₂ atmosphere. Fourier transform infrared (FTIR) spectroscopy (NICOLET 8700, Thermo Nicolet Corporation) tests were conducted to verify the chemical composition of the powders calcined at 400 °C with KBr as the reference. The solid-state ²⁹Si magic angle spinning nuclear magnetic resonance (MAS NMR) spectra of the powders calcined at 400 °C were recorded at 79.48 MHz on a NMR spectrometer (AVANCE III 400 MHz, Bruker). CO₂ (purity = 99.99%) from the Nanjing Special Gases Company was used to evaluate the microstructure of the powders *via* the gas adsorption method. N₂ adsorption–desorption isotherms at 77 K and CO₂ adsorption isotherms at 298 K were conducted with a physical gas adsorption instrument (ASAP 2460 and ASAP 2020, Micromeritics). Prior to the measurements, samples were degassed under vacuum at 373 K for 12 h.

2.3. Membrane preparation and characterization

The organosilica sols were diluted to the same Si concentration (0.17 mol·L⁻¹) and then used for dip-coating on γ-Al₂O₃ mesoporous membranes (pore diameter of 3–5 nm). To avoid the effect of dusts, coating was performed under clean room condition. Subsequently, the coated membranes were dried in a humidity chamber (25 °C, 20% RH) for 3 h. Finally, the membranes underwent the same thermal treatment as described above.

Cross-sections of the prepared membranes were visualized by scanning electron microscopy (SEM, LEO1530VP) with an accelerating voltage of 15 kV. Single gas permeation tests were conducted with a dead-end setup. Gas permeances of the organosilica membranes were measured at 200 °C under a transmembrane pressure of 0.3 MPa. Membranes were tested using various gases with different kinetic diameters, including He, H₂, CO₂, N₂, CH₄ and SF₆. For each membrane, its gas permeance was measured for three times at a time interval of 10 min. The gas permselectivity is equal to the permeance ratio between two gases.
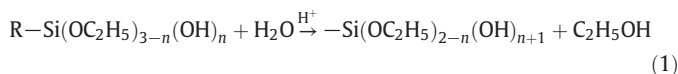
3. Results and Discussion

3.1. Particle size distributions of organosilica sols
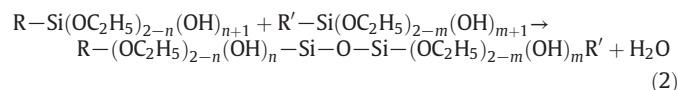
Organosilica sols were synthesized through acid-catalyzed hydrolysis and condensation reaction. In hydrolysis reaction, the ethoxy groups (—OC₂H₅) of BTESE are transformed into hydroxyl groups (—OH), then the products of the hydrolysis reaction

condense together. —Si—O—Si— networks are formed in the condensation reaction [30]. The hydrolysis and condensation reactions of BTESE can be described as follows:

Hydrolysis

$$R-Si(OC_2H_5)_{3-n}(OH)_n + H_2O \xrightarrow{H^+} -Si(OC_2H_5)_{2-n}(OH)_{n+1} + C_2H_5OH \tag{1}$$

Condensation

$$R-Si(OC_2H_5)_{2-n}(OH)_{n+1} + R'-Si(OC_2H_5)_{2-m}(OH)_{m+1} \rightarrow$$
$$R-(OC_2H_5)_{2-n}(OH)_n-Si-O-Si-(OC_2H_5)_{2-m}(OH)_m R' + H_2O \tag{2}$$

where R and R′ represent the organic groups together with other parts, and m and n can be 0, 1, or 2.

Because the improvement of particle size highly depends on the extent of condensation reaction, a careful control of the operational parameters by adjusting the water ratio, acid ratio and solvent ratio in the condensation process is critical in yielding a sol with suitable and narrow particle size distribution [6,15].

Fig. 1 describes the particle size distributions of the synthesized organosilica sols with different water ratios. A homogeneous organosilica sol (sol 1) with clear and transparent appearance was obtained at a molar ratio of 1:13.08:2.29:0.04 for BTESE:EtOH:H₂O:H⁺. Sol 1 has a unimodal particle size distribution within 1.6–20 nm and a mean particle size of 3.3 nm. Another organosilica sol (sol 2) synthesized with low water ratios [$n(H_2O):n(BTESE) = 5.56$] exhibits a similar unimodal particle size distribution ranging from 1.9 to 43 nm and the mean particle size is larger (5.4 nm) compared with that of sol 1. It suggests that increasing water ratios can increase the particle sizes of organosilica sols under unimodal particle size distributions. This observation is consistent with the previous finding [29]. However, further increasing the water ratios causes bimodal particle size distributions (sol 3 and sol 4). Two core-level peaks of the particle size distribution for sol 3 are at 1.6 and 7.4 nm, respectively. Sol 4 has relatively larger particle size than sol 3. The polydispersity of particle sizes can be explained by the high reaction rate due to the high water content at high water ratios. In Eq. (1), water is one of the reactants in the hydrolysis step of BTESE. According to the reaction kinetics, a higher dosage of water leads to a higher reaction rate.

Fig. 2 shows the effects of acid ratios on the particle size distributions of organosilica sols. The organosilica sols synthesized at different acid

ratios (hydrolysis ratio 3.44 and solvent ratio 13.08) show similar particle size distributions [Fig. 2(a)]. Particle size distribution results of sol 5–8 show that all these sols are unimodal with mean particle sizes of 3.6–3.8 nm and that the acid ratios have little effect on the particle size distributions of the sols. However, when the water ratio and solvent
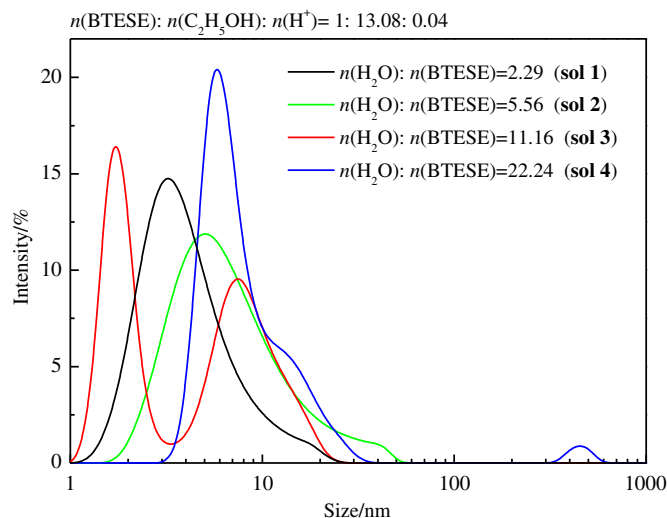

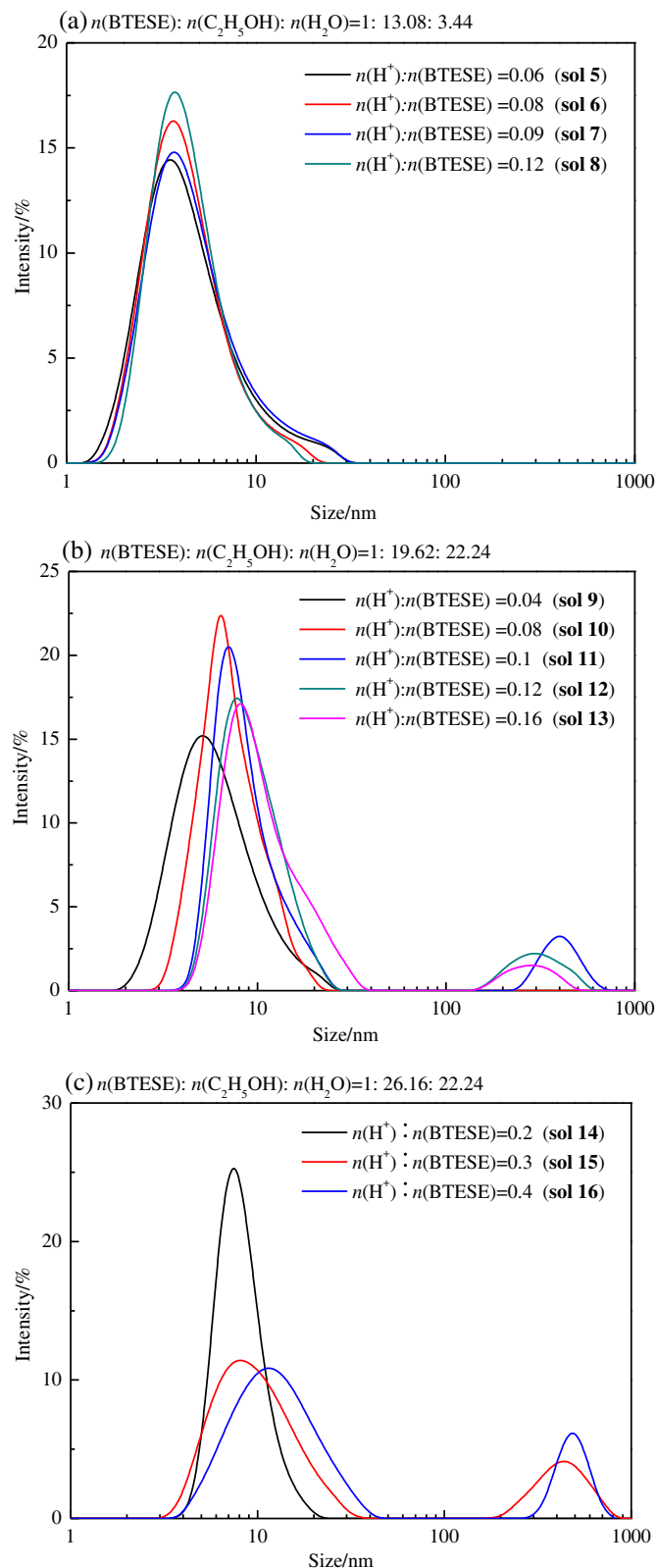**Fig. 2.** Particle size distributions of the organosilica sols formed at different acid ratios.

Fig. 1. Particle size distributions of the organosilica sols formed at different hydrolysis ratios.

ratio increase, the acid ratio has a decisive effect on the particle size distributions of organosilica sols and the particle size increases with the increase of the acid ratio [Fig. 2(b)]. A similar tendency was observed by Kreiter *et al.* [29]. Sol 9 and sol 10 synthesized at lower acid ratios (0.04 and 0.08) have unimodal and narrow particle size distributions and the mean particle sizes are 5.1 and 6.3 nm, respectively, while sols 11–13 synthesized at higher acid ratios [$n(H^+):n(BTESE) \geq 0.1$] have bimodal particle size distributions with core-level peaks at around 8 nm and shoulder peaks at several hundred nanometers. The intensity signal in the larger size region (>100 nm) indicates that some particles aggregate into clusters. The aggregation can be explained by the fast reaction rate due to the large amount of catalyst.

A similar change trend was observed when $n(BTESE):n(EtOH):n(H_2O) = 1:26.16:22.24$ [Fig. 2(c)]. Sol 14 with a lower acid ratio (0.2) has a mean particle size of 7.1 nm and a relatively narrow particle size distribution (4.5 to 18.06 nm). Sol 15 and sol 16 with higher acid ratios (0.3 and 0.4) show bimodal particle size distributions. Meanwhile, acid (HNO_3) acts as the catalyst of the hydrolysis reaction of BTESE as shown in Eq. (1). It is noteworthy that the effects of the acid ratio on the particle size distribution of BTESE-derived sols are obviously different under water-poor and water-rich conditions. Under water-poor conditions, the acid ratio has little effects on the particle size [Fig. 2(a)], while under water-rich conditions, high acid ratios result in large particle sizes [Fig. 2(b) and (c)]. There are 6 hydrolysable ethoxy groups in each BTESE molecule. Thus when the water ratio is below 6 (*e.g.*, $n(H_2O):n(BTESE) = 3.44$), the hydrolysis reaction of BTESE is restricted, though the acid ratio increases. When the water ratio is higher than 6 (*e.g.*, $n(H_2O):n(BTESE) = 22.24$), the hydrolysis reaction becomes acid ratio dependent. Hence, high acid ratios lead to the increase of particle sizes.

Fig. 3 exhibits the particle size distributions of the organosilica sols synthesized at different solvent ratios (water ratio 22.4 and acid ratio 0.04). The sols synthesized at lower solvent ratios (6.54 and 13.08) have bimodal particle size distributions with core-level peaks at several nanometers and shoulder peaks at hundreds nanometer, while the sols synthesized at higher solvent ratios (19.62 and 26.16) show unimodal particle size distributions and the corresponding mean particle sizes are 5.1 and 4.1 nm, respectively. Higher solvent ratios resulting in narrower particle size distributions could be explained by the following two mechanisms. First, high solvent ratios cause low reactivity and thus small particle sizes. Second, high solvent ratios lead to high dispersion of the products from the hydrolysis and condensation reaction, preventing particle aggregation into clusters.
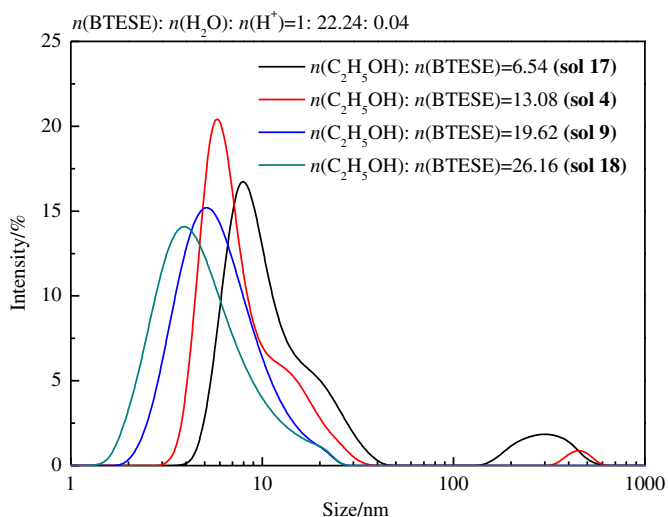
3.2. Organosilica powders after thermal treatment

All the BTESE-derived sols show clear and transparent appearances without any gelation. Since the support layer has a pore size of 3–5 nm, sols with mean particle sizes larger than 5 nm and uniform particle size distributions are desirable for dip-coating. Sol 9 and sol 14 were selected for membrane preparation due to their narrow particle size distributions and suitable mean particle sizes (5 and 7 nm, respectively). Sol 9 and sol 14 were further denoted as BTESE5 and BTESE7, respectively. Powders BTESE5 and BTESE7 have similar thermal evolutions under N_2 atmosphere heating from room temperature to 800 °C (Fig. 4). Three-stage mass loss can be clearly observed in the TG curves. In the first stage, a vast mass decline (9.5% and 11.5% for BTESE5 and BTESE7, respectively) was monitored below 250 °C, which can be attributed to the loss of physically adsorbed water and solvent (*i.e.* dehydration and desolvent process). Next, a dehydroxylation step took place at 250–540 °C and caused about 4% mass loss. A gradual decomposition of the organic moieties in the organosilica powders started at 540 °C [31]. Therefore, the thermal treatment of organosilica membranes was selected at a moderate temperature of 400 °C to maintain the organic moiety in the network.

FTIR spectra of the organosilica powders calcined at 400 °C under N_2 atmosphere (Fig. 5) show a dominant peak at around 1020 cm^{-1}, which

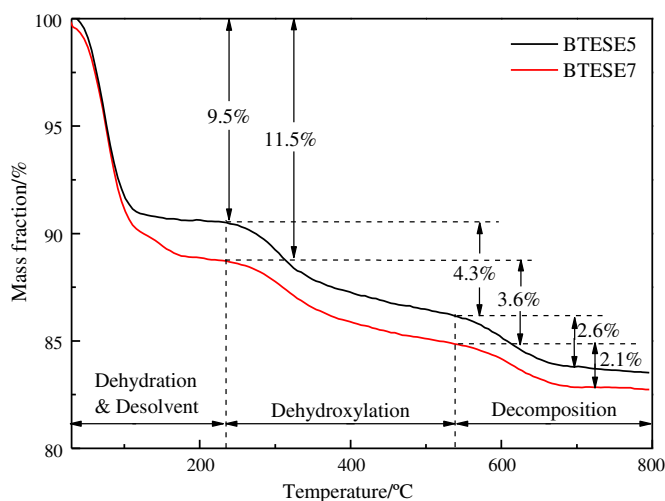**Fig. 4.** Thermogravimetric curves of the organosilica gels.

Fig. 3. Particle size distributions of the organosilica sols formed at different solvent ratios.
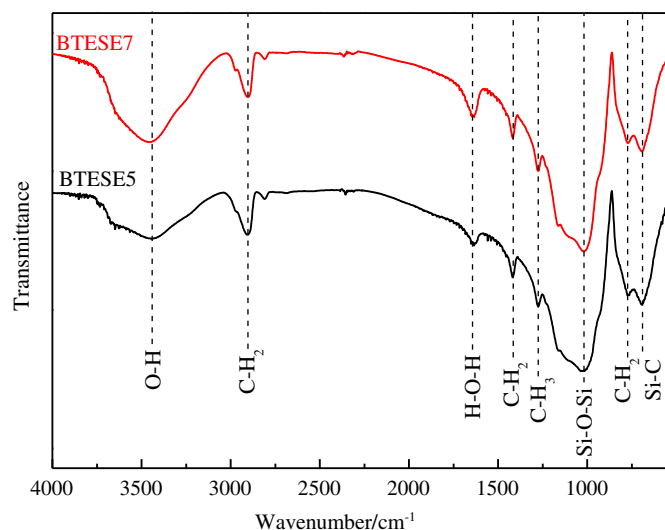
Fig. 5. FTIR spectra of the organosilica powders calcined at 400 °C under N_2 atmosphere.

is corresponding to the asymmetric stretching vibrations of the Si—O—Si bond. The two peaks at approximately 700 and 1410 cm^{-1} correspond to Si—C stretching and C—H (in Si—CH$_2$—CH$_2$—Si) asymmetric bending vibration. The broad band at 3200–3700 cm^{-1} agrees with the stretching vibration of hydroxyl groups in Si—OH (absorption peak: 3450 cm^{-1}) and adsorbed water (absorption peak: 3250 cm^{-1}) [7,32].

Fig. 6 shows ^{29}Si MAS NMR spectra of the organosilica powders calcined at 400 °C under N$_2$ atmosphere. Both powders show apparent signal peaks of the T^n structure (CSi(OSi)$_n$(OH)$_{3-n}$, n = 1, 2 and 3). These peaks can be ascribed to the overlapping signal peaks of the T^2 (CSi(OSi)$_2$OH: approximately at −60) and T^3 (CSi(OSi)$_3$: approximately at −68) structures [32–34], indicating highly branched networks. A negligible broad resonance region of the Q^n structure (Si(OSi)$_n$(OH)$_{4-n}$, n = 2, 3, and 4) occurs in the range of −97 to −110 [32,33], suggesting that almost all organic groups are integral after thermal treatment, which also agrees with the FTIR data.
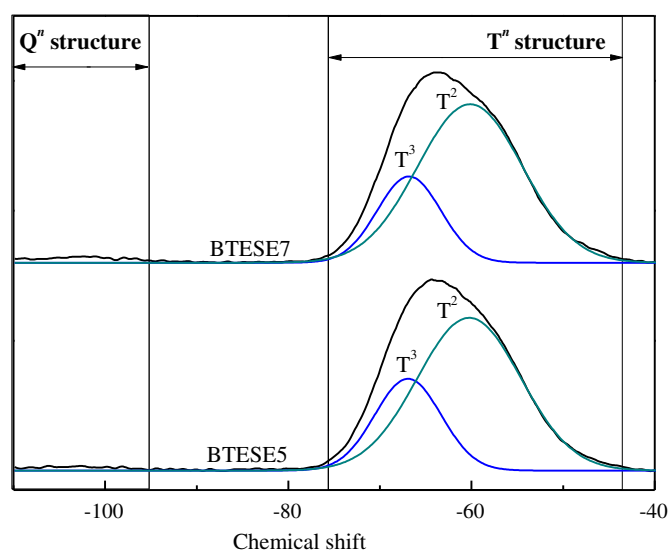

Fig. 6. Solid-state ^{29}Si MAS NMR spectra of the organosilica powders calcined at 400 °C under N$_2$ atmosphere.

Fig. 7 describes the N$_2$ adsorption–desorption and CO$_2$ adsorption isotherms of powder BTESE5 and BTESE7. The type I N$_2$ adsorption–desorption isotherms are observed for the two samples, suggesting that the organosilica powders have microporous structures. The specific surface areas of organosilica powders were calculated by the BET method (based on N$_2$ adsorption–desorption results) and the Dubinin method (based on CO$_2$ uptake data) [8]. The specific surface areas and pore volumes of powders BTESE5 and BTESE7 are displayed in Table 2. Obviously, powder BTESE7 has higher specific surface area and pore volume than powder BTESE5, suggesting that powder BTESE5 has a denser (i.e. less porous) structure compared with powder BTESE7 due to the smaller sol size of BTESE5. Moreover, powder BTESE5 has higher microporosity than powder BTESE7. This may lead to higher gas permselectivity for membrane BTESE5 compared with membrane BTESE7.

3.3. Membrane morphology

Fig. 8 displays the cross-sectional SEM images of membrane BTESE5 and BTESE7. A three layered structure of the membrane, i.e. an α-Al$_2$O$_3$ macroporous support, a γ-Al$_2$O$_3$ mesoporous intermediate layer and an organosilica layer is clearly observed. The two membranes have very similar intermediate and top 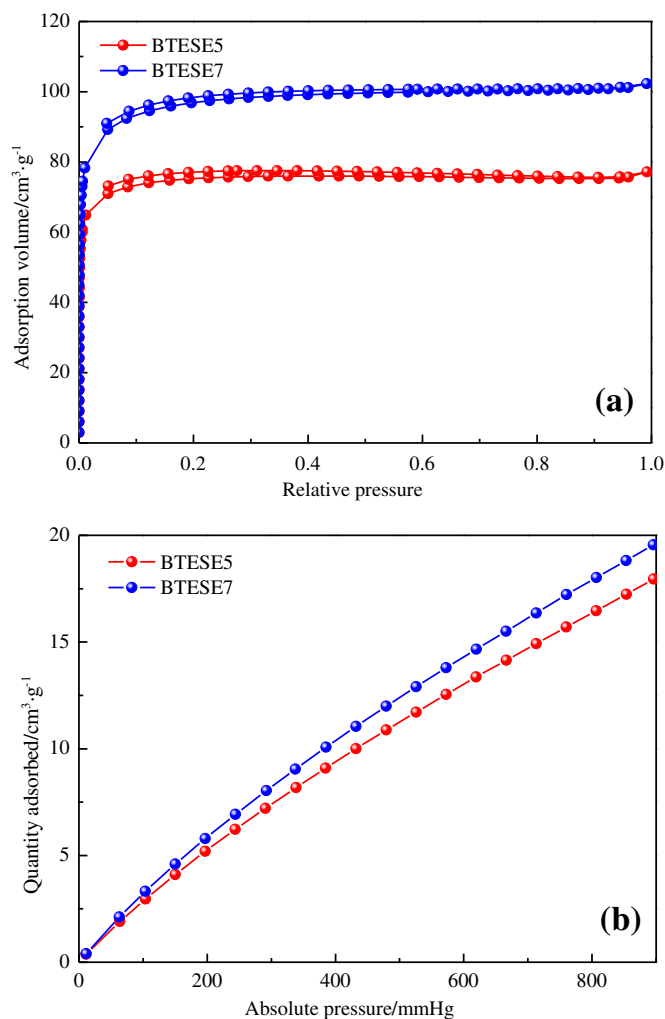selective layers. The thickness of the intermediate layer is around 1.5 μm, while the thickness of the top selective layer is about 130 nm.

Fig. 7. N$_2$ adsorption–desorption (a) and CO$_2$ adsorption (b) isotherms of the organosilica powders calcined at 400 °C under N$_2$ atmosphere. 1 mmHg = 133.322 Pa.

3.4. Performance evaluation of organosilica membranes

Single gas (including He, H$_2$, CO$_2$, N$_2$, CH$_4$ and SF$_6$) permeances of the organosilica-coated membranes were measured at 200 °C (Fig. 9). Gas permeances of the orgaosilica membranes show good reproducibility under the test condition (200 °C and 0.3 MPa). The experimental error was as low as ~1%. It can be seen that the single gas permeance of the organosilica membranes decreases as the molecular kinetic diameter increases due to the molecular sieving effect [35]. The organosilica membranes show excellent gas permselectivities (inset in Fig. 9). The H$_2$/CO$_2$, H$_2$/N$_2$ and H$_2$/CH$_4$ permselectivities of membrane BTESE5 are respectively 9.5, 50 and 68, and those of membrane BTESE7 are respectively 7.1, 31 and 46. These results are much higher than the corresponding Knudsen diffusion factors (4.7 for H$_2$/CO$_2$, 3.7 for H$_2$/N$_2$ and 2.8 for H$_2$/CH$_4$). Moreover, membrane BTESE7 has higher gas permeances for all the gases than membrane BTESE5. Particularly, membrane BTESE5 has a H$_2$ permeance of 2.9×10^{-7} mol·m^{-2}·s^{-1}·Pa^{-1}, while the H$_2$ permeance of membrane BTESE7 is as high as 4.2×10^{-7} mol·m^{-2}·s^{-1}·Pa^{-1} due to its more porous structures which is beneficial for gases passing through. These results agree well with the results of gas adsorption.

Desirable membranes for efficient gas separation should have high permeances for small molecules (e.g. H$_2$) and high selectivities

Table 2
Porous structure data of the organosilica powders calcined at 400 °C under N_2 atmosphere

Sample	A_{N_2}/$m^2 \cdot g^{-1}$	A_{CO_2}/$m^2 \cdot g^{-1}$	V_{total}/$m^3 \cdot g^{-1}$	V_{micro}/$m^3 \cdot g^{-1}$	(V_{micro}/V_{total})/%
BTESE5	229	194	0.117	0.102	87.2
BTESE7	298	215	0.156	0.122	78.2

Note: A_{N_2} and A_{CO_2} represent the specific surface area determined from N_2 adsorption desorption and CO_2 adsorption, respectively. V_{total}, V_{micro} and V_{total}/V_{micro} denote total pore volume, micropore volume and microporosity, respectively.
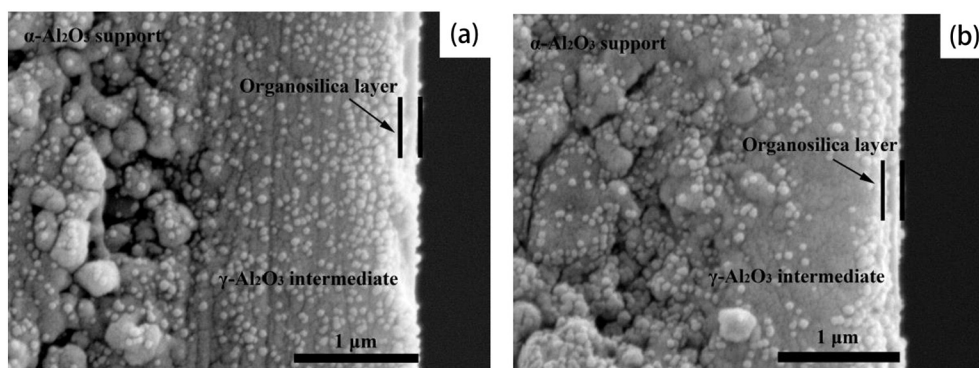

Fig. 8. Cross sectional SEM images of membranes (a) BTESE5 and (b) BTESE7.
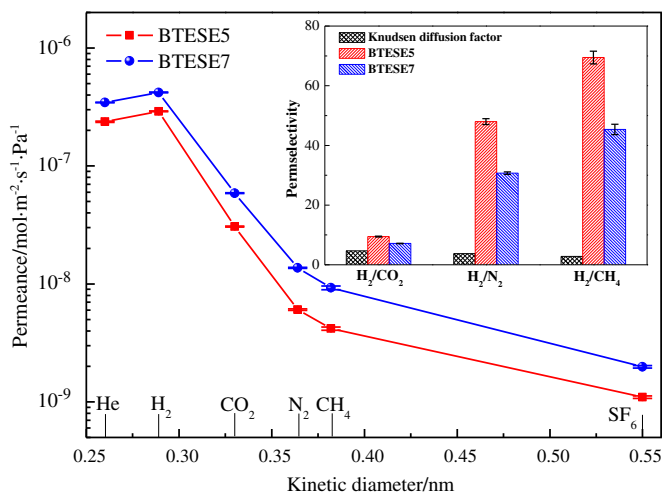

Fig. 9. Single gas permeances and permselectivities (inset) of the organosilica membranes calcined at 400 °C under N_2 atmosphere (measurement temperature 200 °C).
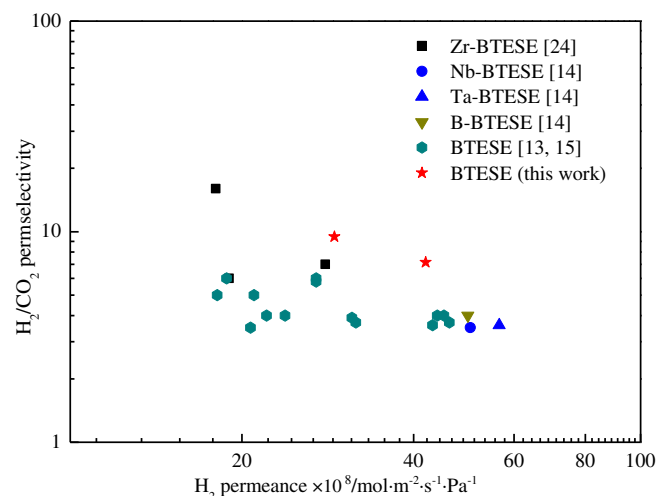

Fig. 10. Performance comparison of the organosilica membranes and other doped organosilica membranes.

for gas pairs (*e.g.*, H_2/CO_2). Fig. 10 presents the performance comparison in the terms of the H_2 permeance and H_2/CO_2 permselectivity of BTESE membranes and doped BTESE membranes measured at 200 °C [13–15,24]. Membranes BTESE5 and BTESE7 show higher H_2/CO_2 permselectivity than that of the BTESE, Nb-BTESE, Ta-BTESE and B-BTESE membranes reported in literature. Compared with the state-of-the-art Zr-BTESE membrane, membranes BTESE5 and BTESE7 have lower H_2/CO_2 permselectivities, but much higher H_2 permeances. Such difference can be attributed to the relatively dense microporous structure of the Zr-BTESE membrane.

4. Conclusions

BTESE-derived organosilica sols with different particle size distributions were systematically investigated by tuning the synthesis parameters, including water ratios, acid ratios and solvent ratios. Organosilica sols with uniform particle size distributions can be well controlled through our facile method. In certain conditions, increasing the water ratio or the acid ratios tends to cause larger sol sizes and bimodal particle size distributions. However, higher solvent ratios lead to smaller sol sizes and unimodal particle size distributions. After thermal treatment at 400 °C, organic groups in powders BTESE5 and BTESE7 are integral. Gas adsorption results demonstrate that powder BTESE5 has a denser structure than powder BTESE7. Membrane BTESE5 shows a relatively high H_2 permeance (2.9×10^{-7} $mol \cdot m^{-2} \cdot s^{-1} \cdot Pa^{-1}$), and high H_2/CO_2, H_2/N_2 and H_2/CH_4 permselectivities (9.5, 50 and 68), which are much higher than the corresponding Knudsen diffusion factors. Moreover, membrane BTESE7 shows better gas permeances but lower permselectivities than membrane BTESE5. Our work offers significant insights into the relationships between sol synthesis parameters, sol sizes and membrane performance.

References

[1] I. Agirre, P.L. Arias, H.L. Castricum, M. Creatore, J.E. ten Elshof, G.G. Paradis, P.H.T. Ngamou, H.M. van Veen, J.F. Vente, Hybrid organosilica membranes and processes: Status and outlook, *Sep. Purif. Technol.* 121 (2014) 2–12.

[2] G.G. Paradis, D.P. Shanahan, R. Kreiter, H.M. van Veen, H.L. Castricum, A. Nijmeijer, J.F. Vente, From hydrophilic to hydrophobic HybSi® membranes: A change of affinity and applicability, *J. Membr. Sci.* 428 (2013) 157–162.

[3] E.J. Kappert, D. Pavlenko, J. Malzbender, A. Nijmeijer, N.E. Benes, P.A. Tsai, Formation and prevention of fractures in sol–gel-derived thin films, *Soft Matter* 11 (2015) 882–888.

[4] H.L. Castricum, R. Kreiter, H.M. van Veen, D.H.A. Blank, J.F. Vente, J.E. ten Elshof, High-performance hybrid pervaporation membranes with superior hydrothermal and acid stability, *J. Membr. Sci.* 324 (2008) 111–118.

[5] X. Ren, K. Nishimoto, M. Kanezashi, H. Nagasawa, T. Yoshioka, T. Tsuru, CO_2 permeation through hybrid organosilica membranes in the presence of water vapor, *Ind. Eng. Chem. Res.* 53 (2014) 6113–6120.

[6] J. Ambati, S.E. Rankin, Reaction-induced phase separation of bis(triethoxysilyl)ethane upon sol–gel polymerization in acidic conditions, *J. Colloid Interface Sci.* 362 (2011) 345–353.

[7] P.H.T. Ngamou, J.P. Overbeek, R. Kreiter, H.M. van Veen, J.F. Vente, I.M. Wienk, P.F. Cuperus, M. Creatore, Plasma-deposited hybrid silica membranes with a controlled retention of organic bridges, *J. Mater. Chem. A* 1 (2013) 5567–5576.

[8] H.L. Castricum, G.G. Paradis, M.C. Mittelmeijer-Hazeleger, R. Kreiter, J.F. Vente, J.E. ten Elshof, Tailoring the separation behavior of hybrid organosilica membranes by adjusting the structure of the organic bridging group, *Adv. Funct. Mater.* 21 (2011) 2319–2329.

[9] R. Xu, S.M. Ibrahim, M. Kanezashi, T. Yoshioka, K. Ito, J. Ohshita, T. Tsuru, New insights into the microstructure-separation properties of organosilica membranes with ethane, ethylene, and acetylene bridges, *ACS Appl. Mater. Interfaces* 6 (2014) 9357–9364.

[10] P.H.T. Ngamou, J.P. Overbeek, H.M. van Veen, J.F. Vente, P.F. Cuperus, M. Creatore, On the enhancement of pervaporation properties of plasma-deposited hybrid silica membranes, *RSC Adv.* 3 (2013) 14241–14244.

[11] H.L. Castricum, G.G. Paradis, M.C. Mittelmeijer-Hazeleger, W. Bras, G. Eeckhaut, J.F. Vente, G. Rothenberg, J.E. ten Elshof, Tuning the nanopore structure and separation behavior of hybrid organosilica membranes, *Microporous Mesoporous Mater.* 185 (2014) 224–234.

[12] H. Nagasawa, N. Matsuda, M. Kanezashi, T. Yoshioka, T. Tsuru, Pervaporation and vapor permeation characteristics of BTESE-derived organosilica membranes and their long-term stability in a high-water-content IPA/water mixture, *J. Membr. Sci.* 498 (2016) 336–344.

[13] H.L. Castricum, H.F. Qureshi, A. Nijmeijer, L. Winnubst, Hybrid silica membranes with enhanced hydrogen and CO_2 separation properties, *J. Membr. Sci.* 488 (2015) 121–128.

[14] H.F. Qureshi, R. Besselink, J.E. ten Elshof, A. Nijmeijer, L. Winnubst, Doped microporous hybrid silica membranes for gas separation, *J. Sol-Gel Sci. Technol.* 75 (2015) 180–188.

[15] H.F. Qureshi, A. Nijmeijer, L. Winnubst, Influence of sol–gel process parameters on the micro-structure and performance of hybrid silica membranes, *J. Membr. Sci.* 446 (2013) 19–25.

[16] M. Kanezashi, K. Yada, T. Yoshioka, T. Tsuru, Design of silica networks for development of highly permeable hydrogen separation membranes with hydrothermal stability, *J. Am. Chem. Soc.* 131 (2009) 414–415.

[17] S.M. Ibrahim, H. Nagasawa, M. Kanezashi, T. Tsuru, Robust organosilica membranes for high temperature reverse osmosis (RO) application: Membrane preparation, separation characteristics of solutes and membrane regeneration, *J. Membr. Sci.* 493 (2015) 515–523.

[18] T. Niimi, H. Nagasawa, M. Kanezashi, T. Yoshioka, K. Ito, T. Tsuru, Preparation of BTESE-derived organosilica membranes for catalytic membrane reactors of methylcyclohexane dehydrogenation, *J. Membr. Sci.* 455 (2014) 375–383.

[19] K.S. Chang, T. Yoshioka, M. Kanezashi, T. Tsuru, K.L. Tung, A molecular dynamics simulation of a homogeneous organic–inorganic hybrid silica membrane, *Chem. Commun.* 46 (2010) 9140–9142.

[20] M. Kanezashi, M. Kawano, T. Yoshioka, T. Tsuru, Organic–inorganic hybrid silica membranes with controlled silica network size for propylene/propane separation, *Ind. Eng. Chem. Res.* 51 (2012) 944–953.

[21] M. Kanezashi, K. Yada, T. Yoshioka, T. Tsuru, Organic–inorganic hybrid silica membranes with controlled silica network size: Preparation and gas permeation characteristics, *J. Membr. Sci.* 348 (2010) 310–318.

[22] L. Meng, M. Kanezashi, J. Wang, T. Tsuru, Permeation properties of BTESE–TEOS organosilica membranes and application to O_2/SO_2 gas separation, *J. Membr. Sci.* 496 (2015) 211–218.

[23] H. Qi, H. Chen, L. Li, G. Zhu, N. Xu, Effect of Nb content on hydrothermal stability of a novel ethylene-bridged silsesquioxane molecular sieving membrane for H_2/CO_2 separation, *J. Membr. Sci.* 421–422 (2012) 190–200.

[24] M. ten Hove, A. Nijmeijer, L. Winnubst, Facile synthesis of zirconia doped hybrid organic inorganic silica membranes, *Sep. Purif. Technol.* 147 (2015) 372–378.

[25] H. Song, S. Zhao, J. Chen, H. Qi, Hydrothermally stable Zr-doped organosilica membranes for H_2/CO_2 separation, *Microporous Mesoporous Mater.* 224 (2016) 277–284.

[26] H. Song, S. Zhao, J. Lei, C. Wang, H. Qi, Pd-doped organosilica membrane with enhanced gas permeability and hydrothermal stability for gas separation, *J. Mater. Sci.* 51 (2016) 6275–6286.

[27] Z. Li, Y. Wang, J. Shen, W. Liu, X. Sun, The measurement system of nanoparticle size distribution from dynamic light scattering data, *Opt. Lasers Eng.* 56 (2014) 94–98.

[28] Z. Li, S.H. Tolbert, D.A. Loy, Hybrid organic–inorganic membranes from size exclusion deposition of fluorescent, octylene-bridged polysilsesquioxane particles, *J. Non-Cryst. Solids* 403 (2014) 88–96.

[29] R. Kreiter, M.D.A. Rietkerk, H.L. Castricum, H.M. van Veen, J.E. ten Elshof, J.F. Vente, Evaluation of hybrid silica sols for stable microporous membranes using high-throughput screening, *J. Sol-Gel Sci. Technol.* 57 (2011) 245–252.

[30] B. Díaz-Benito, F. Velasco, F.J. Martínez, N. Encinas, Hydrolysis study of bis-1,2-(triethoxysilyl)ethane silane by NMR, *Colloids Surf. A Physicochem. Eng. Asp.* 369 (2010) 53–56.

[31] E.J. Kappert, H.J.M. Bouwmeester, N.E. Benes, A. Nijmeijer, Kinetic analysis of the thermal processing of silica and organosilica, *J. Phys. Chem. B* 118 (2014) 5270–5277.

[32] K. Yamamoto, J. Ohshita, T. Mizumo, T. Tsuru, Efficient synthesis of SiOC glasses from ethane, ethylene, and acetylene-bridged polysilsesquioxanes, *J. Non-Cryst. Solids* 408 (2015) 137–141.

[33] M. Imamoglu, D. Pérez-Quintanilla, I. Sierra, Bifunctional periodic mesoporous organosilicas with sulfide bridges as effective sorbents for Hg(II) extraction from environmental and drinking waters, *Microporous Mesoporous Mater.* 229 (2016) 90–97.

[34] D.A. Loy, K.A. Obrey-DeFriend, K.V. Wilson Jr., M. Minke, B.M. Baugher, C.R. Baugher, D.A. Schneider, G.M. Jamison, K.J. Shea, Influence of the alkoxide group, solvent, catalyst, and concentration on the gelation and porosity of hexylene-bridged polysilsesquioxanes, *J. Non-Cryst. Solids* 362 (2013) 82–94.

[35] H.R. Lee, M. Kanezashi, Y. Shimomura, T. Yoshioka, T. Tsuru, Evaluation and fabrication of pore-size-tuned silica membranes with tetraethoxydimethyl disiloxane for gas separation, *AIChE J.* 57 (2011) 2755–2765.